Biosensors and Bioelectronics: X 19 (2024) 100487

Contents lists available at ScienceDirect

Biosensors and Bioelectronics: X

journal homepage: www.journals.elsevier.com/biosensors-and-bioelectronics-x

Metal-organic frameworks as an active substrate for cell-interaction studies and cell-on-a-chip platforms

Huijie Jiang [a,1], Ziyu Gao [b,c,1], Claudia Lubrano [b,c], Claudia Latte Bovio [d,e], Henning Bommes [a], Andrea Kauth [a], Lea Baumann [a], Bo Cheng [a], Divagar Murugan [a], Joachim Knoch [f], Rainer Waser [g,h], Sven Ingebrandt [a], Francesca Santoro [b,c,d], Vivek Pachauri [a,*]

[a] Institute of Materials in Electrical Engineering 1, RWTH Aachen University, Sommerfeldstrasse 24, 52074 Aachen, Germany
[b] Neuroelctronic Interfaces Teaching and Research Area, RWTH Aachen University, 52074 Aachen, Germany
[c] Institute for Biological Information Processing – Bioelectronics, IBI-3, Forschungszentrum Jülich GmbH, 52428 Aachen, Germany
[d] Tissue Electronics, Istituto Italiano di Tecnologia, 80125 Naples, Italy
[e] Dipartimento di Chimica, Materiali e Produzione Industriale, Università di Napoli Federico II, 80125, Naples, Italy
[f] Institute of Semiconductor Electronics, RWTH Aachen University, 52074 Aachen, Germany
[g] Institute of Materials in Electrical Engineering II, RWTH Aachen University, 52074 Aachen, Germany
[h] Institute of Materials in Electrical Engineering and Information Technology (IWE2), RWTH Aachen University, 52056 Aachen, Germany

ARTICLE INFO

Keywords:
Metal-organic frameworks
Cell-substrate interaction
Bioelectronics
Biocompatibility
Electrical cell-substrate impedance spectroscopy
Cell-culture assay

ABSTRACT

Metal-organic frameworks (MOFs) are an emerging class of nanomaterials with immense biomedical potential for their unique interactions with biological and organic materials. In this work, we select two candidate two-dimensional (2D) MOF systems based on Fe^{3+} and Ni^{2+} metal centers and 2-aminoterephthalate acid ligand (Fe-MOF and Ni-MOF) and evaluate their performance as an active interface for study of cell-interactions. 2D Fe-MOF and Ni-MOF were synthesized onto hydroxyl-modified gold and glass substrates using a layer-by-layer liquid-phase-epitaxy (LbL-LPE) growth at room temperature and used as active substrates (Fe-MOF/glass, Fe-MOF/Au, Ni-MOF/glass and Ni-MOF/Au, respectively) for MTT cell-proliferation and reactive oxygen species tests using the PC-12 cell-line in order to investigate the biocompatibility. Immunostaining and morphological analyses of PC-12 cells on MOF interfaces suggested a stronger cell-substrate interaction in comparison to glass and were further characterized using the Electrical Cell-substrate Impedance Sensing (ECIS) technique, here for the first time, employed to study cell attachment, spreading and proliferation on 2D Fe-MOF. The 2D Fe-MOF showed superior long-term stability in cell culture medium by recording impedance over 24 h, crucial to monitor cell-dynamics at a solid-liquid interface. A significant increase of interfacial impedance was observed in ECIS, due to PC-12 cells adhering onto 2D Fe-MOF, which was also confirmed by the focused ion beam etching followed by scanning electron microscopy. Our novel findings, therefore, suggest 2D MOFs as highly suitable platform for the study of cell-related interactions using electrical techniques and potentially pave the way for future use of MOFs for bioelectronics and biosensor applications.

1. Introduction

Living-systems, such as cells, actively interact with their surroundings, which strongly influence their sustenance and growth (Miller 1973). The growth substrates or templates are one of the critical external factors that have a decisive influence on the cell growth and sustenance and overall behaviour. Cell-substrate interactions therefore attract an immense interest in the field of cell-biology and have been at the center of the development of various cell-based assays. In addition, cell-substrate interactions are also in the focus of research for future applications in bioelectronics, biological implants and tissue regeneration (Ermis et al., 2018; Vandrovcová and Bacáková 2011; Wang et al., 2008). For example, the study of interactions between cells and substrates can provide valuable insights on how to design novel materials or substrates that promote cell adhesion, growth and differentiation (Ermis et al., 2018; Rajendran et al., 2023; Sniadecki et al., 2006; Vandrovcová

* Corresponding author.
E-mail address: pachauri@iwe1.rwth-aachen.de (V. Pachauri).
[1] Equal contribution.

https://doi.org/10.1016/j.biosx.2024.100487
Received 14 January 2024; Received in revised form 16 March 2024; Accepted 7 May 2024
Available online 11 May 2024

and Bacáková 2011). The design of optimal cell-substrate interfaces, therefore, are not only critical to study the fundamental of cellular-life, but also to develop or improve technique for their studies. One of the well-established techniques for examining cell-substrate interactions is Electrical Cell-Substrate Impedance Sensing (ECIS), with advantages of being noninvasive, real-time and offering long-term monitoring of cell dynamics (Hedayatipour et al., 2019; Hempel et al., 2021; Hong et al., 2011; Liu et al., 2014; Szulcek et al., 2014; Wegener et al., 2000; Xu et al., 2016). Over past few decades, ECIS has seen significant advances together with the development in microfabrication of dedicated device platforms using metal or semiconductor materials as active substrates (Hempel et al., 2021; Wegener et al., 2000). Other than the development of planar metal-electrodes and advanced microelectrode-arrays with sophisticated materials and geometries, the use of standard silicon technology towards realization of dedicated semiconductor chips for cell-based bioassays, stimulations and recordings can be considered as significant milestones in ECIS (Ghafar-Zadeh et al., 2010; Lin et al., 2006; Vinzons et al., 2022). Thereby, physical properties of an active substrate and related transduction mechanism come into consideration, in the design of advanced cell-substrate interfaces and remain an area of active exploration.

Conductive organic materials based on poly (3,4-ethylenedioxythiophene)polystyrene sulfonate (PEDOT:PSS), have become a standard for realization of biological interfaces with lower interfacial impedance (Hempel et al., 2021; Kavand et al., 2022; Pitsalidis et al., 2022; Rossetti et al., 2021). ECIS platforms based on conductive organic polymers such as PEDOT:PSS, while offering inherent advantages of superior electrical characteristics, also suffer a few critical drawbacks. Interfacial instabilities and electrochemical drifts related to water-soluble materials and interfaces based on PEDOT:PSS pose a significant challenge for designing bioelectronics platforms for sustained operation (Chen et al., 2020; Li et al., 2022; Marks et al., 2022; Nawaz et al., 2021). Countering such disadvantages by chemically substituted and physically modified materials and interfaces so far provides only incremental gains and remains far from realization of reliable interfaces. Therefore, it is of critical importance to investigate alternative material systems in order to address the drawbacks related to material instability in biological media in order to design versatile, long-term stable interfaces with excellent electrical characteristics.

Metal-organic frameworks (MOFs), which are also known as porous coordination polymers (PCPs), constitute ordered crystalline lattices through coordination of metal clusters with organic ligands (Diring et al., 2017; Furukawa et al., 2013; Long and Yaghi 2009; Zhou and Kitagawa 2014). Such metal-organic coordination, due to virtually unlimited combinations to construct porous crystalline solids in dimensions ranging from nano-to micron-scale, together with adjustable electrical and optical characteristics exhibit tremendous potential in numerous areas including gas separation/storage, catalysis, energy storage/conversion and sensor applications (Cui et al., 2016; Kreno et al., 2012; Kuppler et al., 2009; Liao et al., 2018). The development of MOFs so far, was mostly driven by exploiting and optimizing their unique characteristics for chemistry-related applications where high surface-areas/porosity, customized topography and highly accessible functional groups are of key-interest. Interestingly, MOFs also found their use in cell-biology applications as promising material system for drug-delivery, bio-imaging and similar biomedical studies (Gao et al., 2020; Horcajada et al., 2012; McKinlay et al., 2010; Vodyashkin et al., 2023). Recently, researchers deposited 2D Al-based MIL-53 (MIL = Material Institute Lavoisier) onto polymeric substrates to use it as scaffolds for the growth of C2C12 cell-line (an immortalized mouse myoblast cell line), which exhibited greater serum protein adsorption, retention, and replenishment capabilities than conventional cell-culture scaffolds (Katayama et al., 2022). Particularly, C2C12 cells cultured on MIL-53 (Al) films loaded with serum proteins demonstrated exceptional adhesion, morphology, and proliferation, even in the absence of serum protein in the medium. ZIF-8 (ZIF = Zeolitic imidazolate framework) modified polypropylene membranes have been applied as a biomimetic cell-culture platform to improve guided bone regeneration (Ejeian et al., 2020). Therefore MOFs are emerging as potential material-systems for advanced cell-related studies which requires careful examinations such as varying stability of MOFs in complex extracellular matrix media and thorough analyses of biocompatibility towards different cell lines (Hanke et al., 2012).

This work, reports on cell-substrate interactions by utilizing different 2D MOFs, as active interfaces by utilizing the well-established ECIS technique to electrochemically test the cell-substrate adhesion complemented by cell-biology experiments to ascertain the biocompatibility. In brief, we selected two 2-aminoterephthalate acid (BDC–NH_2)–based MOFs (namely Fe-MOF and Ni-MOF) constructed of Fe^{3+} or Ni^{2+} via coordination reactions, as active 2D interfaces for investigating the interactions with the PC-12 neuroblastoma cell line. As shown in Fig. 1, ~20 nm Fe-MOF was deposited on 11-MUD (11-Mercapto-1-undecanol) functionalized gold (Au) electrodes through a layer-by-layer liquid phase epitaxy (LbL-LPE) method (Semrau et al., 2021). These Fe-MOF coated Au electrodes were wire-bonded and encapsulated on printed circuit boards (PCB). Then, PC-12 cells were seeded onto the 2D Fe-MOF substrates and monitored by electrochemical impedance spectroscopy (EIS) inside an incubator for up to 24 h. The 2D Fe-MOF exhibited excellent long-term electrochemical stability in a cell-culture medium. A superior biocompatibility to PC-12 cells was confirmed by conducting 3-(4,5-dimethylthazolk-2-yl)-2,5-diphenyl tetrazolium bromide-based cell proliferation assays and analyzing the reactive ion species. While the biocompatibility of the 2D Fe-MOF is attributed to the non-toxic constituents and abundant surface functional groups, the PC-12 cell culture showed distinct cell-attachments, spreading and proliferation over 24 h. Long-term EIS characterizations of PC-12 cells with 2D Fe-MOF modified Au electrodes showed a distinct change in the impedance related to cell attachment, spreading and proliferation stages, suggesting immense potential of MOF-based interfaces for conducting cell-related studies and applications.

2. Materials and methods

All reagents, chemicals and solvents used in this study were used without further purification except the chemicals and solvents used for cell culture, which were further processed by filtration and sterilization.

2.1. Realization of 2D MOF at gold electrodes

$FeCl_3{\cdot}6H_2O$, $NiCl_2{\cdot}6H_2O$ and 2-aminoterephthalic acid (BDC-NH_2), purchased from Sigma-Aldrich Chemie GmbH (Germany), were used for the synthesis of 2D Fe-MOF and Ni-MOF, respectively. $FeCl_3{\cdot}6H_2O$ was dissolved in deionized (DI) water with a concentration of 1 mM, while the BDC-NH_2 solution with the same concentration was prepared by dissolving it in an aqueous 10 mM KOH solution. In contrast, the 1 mM $NiCl_2{\cdot}6H_2O$ and 1 mM BDC-NH_2 solutions were prepared in ethanol for the synthesis of Ni-MOF. Prior to the deposition of Fe-MOF or Ni-MOF on Au substrates, 10 nm Ti and 100 nm Au were deposited on 4′ glass wafers through thermal evaporation and diced into chips with sizes 1.5 × 1.0 cm^2. Then, these Au chips were cleaned by acetone and isopropanol in an ultrasonication bath, which was followed by surface functionalization using 1 mM 11-Mercapto-1-undecanol (11-MUD, Sigma-Aldrich Chemie GmbH) ethanolic solution for 24 h (Dhanapala et al., 2023). Then, the epitaxial growth of 2D Fe-MOF on Au substrates was performed using the LbL-LPE technique (Semrau et al., 2021). To avoid too many manual steps in the LbL-LPE protocol and to improve reproducibility, we developed an automated dip coater (Fig. S1, supporting information file, **SI**), which was then deployed for programmable synthesis of 2D MOFs. In the LbL-LPE process, typically, 11-MUD functionalized Au substrates were submersed into the $FeCl_3$ solution for 10 min, followed by a rinsing step to wash away unreacted precursors. Afterwards, these substrates were dipped into the BDC-NH_2 solution for

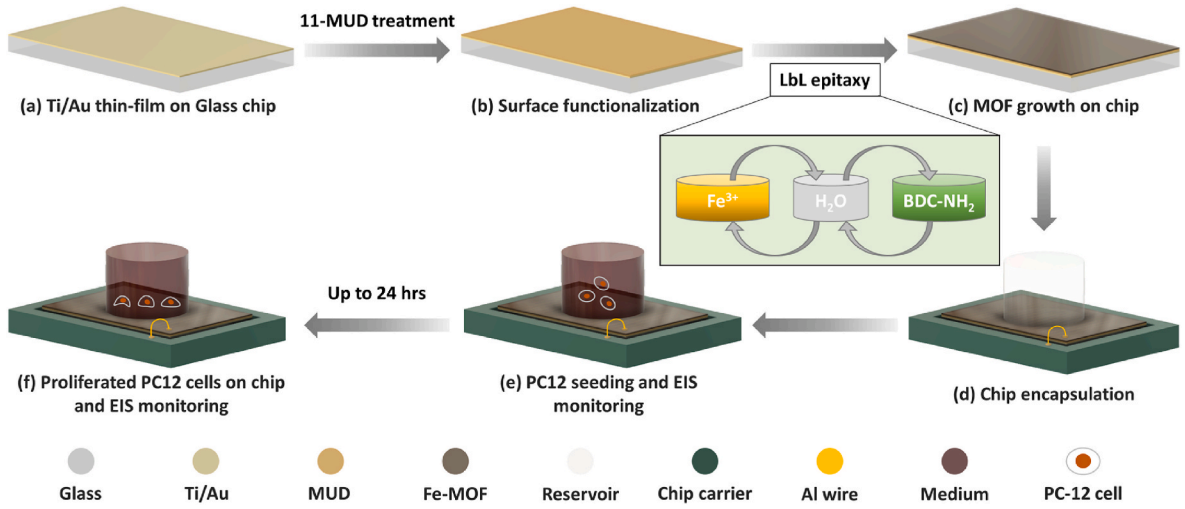

Fig. 1. Schematic illustration representing the integration of 2D Fe-MOF thin films for performing ECIS with PC-12 cells. (a) Ti/Au coated glass chips were diced from a 4 inch wafer and cleaned. (b) The chips were functionalized with 11-MUD molecules to provide chemical anchors for the epitaxy growth of MOFs in a layer-by-layer (LbL) epitaxy approach, where chips are dipped into metal clusters (Fe^{3+} or Ni^{2+}), rinsing solution (H_2O) and organic ligand solution (BDC-NH_2) repeatedly, (c) After LbL-LPE, the 2D MOF thin films with desired thickness were grown on the chips. (d) The 2D MOF coated chips were placed onto a chip-carrier followed by wire-bonding and an encapsulation procedure to create a mL volume reservoir for the cell-culture. (e, f). Start of the seeding procedure of PC-12 cells on the encapsulated chip and long-term EIS monitoring.

another 10 min. Similarly, the second washing step was performed to remove organic precursor residues. This procedure was repeated multiple times resulting in longer protocols which were steadily performed by our dip coater. After twenty deposition cycles, the final 2D Fe-MOF substrates were dried at 85°C and stored in an N_2 chamber for further characterizations and experiments. For Fe-MOF and Ni-MOF thin film deposition on glass substrates, oxygen plasma treatment was employed instead of MUD functionalization, while the growth parameters remained same as for the Au substrates. For the patterning of Fe-MOF thin films on Au substrates please refer to Fig. S2 in **SI**.

2.2. PC-12 cell culture on 2D MOF

PC-12 Adh cells (ATCC, CRL1721.1, US) were used for biocompatibility and ECIS experiments. Gibco RPMI-1640 Medium was used for PC-12 culture, supplemented with 2 mM L-Glutamine (25,030,024, ThermoFisher Scientific, US), 10 v/v% Horse inactivated serum (Horse Serum, Donor Herd, USA origin, Heat inactivated, H1138), 5 v/v%, Fetal bovine serum (FBS, Gibco Qualified, 10,270–106, US) and 1 v/v% Penicillin−Streptomycin (PS, Life Technologies, 15,140–122, Germany).

For the PC-12 cell culture on the 2D MOFs, all samples underwent 1 h UV sterilization or were rinsed with 70% ethanol for sterilization and thereafter poly-L-lysine coating (PLL, Sigma-Aldrich, Germany) or collagen IV from human placenta (Sigma-Aldrich, Germany) coating on the MOFs to improve cell adhesion. Typically, 0.1 mg/mL PLL or 1 mg/mL collagen aqueous solution were utilized to functionalize the MOF surfaces at room temperature for 1 h. Then, they were washed thoroughly with sterile distilled water. Finally, PC-12 cells were plated on Fe-MOF thin film substrates and incubated at 37 °C for 24 h (5% CO_2 and 95% humidity).

2.3. Immunostaining experiments

All samples for immunostaining were coated with collagen IV. The immunostaining was carried out after 24-h of cell culture. To fix the cells, culture medium was first removed and samples were rinsed three times with PBS (pH7.4, ThermoFischer Scientific, US). Then, 4 w/v% paraformaldehyde (PFA, ThermoFischer Scientific, US) was added to cover samples surfaces for 15min at room temperature, followed by a PBS washing (*x*3) to remove excessive PFA. The cell membrane was then permeabilized with 0.1 w/v% Triton x-100 for 15 min at room temperature. After another PBS wash (*x*3), unspecific protein binding sites were saturated with blocking buffer (5 wt% bovine serum albumin in PBS, Gibco, New Zealand) for 1 h.

In order to stain the focal adhesion areas, samples were incubated with paxillin (Y113, rabbit, Ab32084, Abcam, UK) for 1 h, and then washed with blocking buffer. Subsequently, samples were further incubated with anti-rabbit-Alexa Fluor 488 (Goat, A11034, ThermoFisher Scientific, US) for 1 h. Actin filaments were located with phalloidin-iFluor 647 Reagent (ab176759, Abcam, UK) for 40 min, and then rinsed with PBS (*x*3). Nuclei were visualized with Hoechst 33,342 (H3570, ThermoFisher Scientific, US) for 10 min, and then rinsed with PBS (*x*3). The staining procedure was carried out at room temperature, immunostained samples were finally mounted with fluorescence mounting medium (Dako Agilent, Germany) and stored at 2–8 °C for microscopy.

2.4. Laser scanning confocal microscopy and morphological analysis

After immunostaining, samples were visualized with a laser scanning confocal microscope (LSM880, Zeiss, Germany). Fluorescence excitation was carried out with lasers at 405 nm (for nucleus), 488 nm (for paxillin) and 633 nm (for F-actin) and images were taken at room temperature using a 40× objective with oil immersion.

The cellular morphology was analysed with the Fiji software (ImageJ). The finalized data were plotted and presented by analyzing cell area, circularity, roundness, perimeter and aspect ratio. A circularity value of 1.0 indicates a perfect circle while a decreasing value indicates an increasingly elongated polygon. The roundness gives a value directly relative to the aspect ratio. Circularity and roundness were calculated using the following equations:

$$Circularity = \frac{4\pi * Area}{Perimeter^2} \quad (1)$$

$$Roundness = \frac{4 * Area}{\pi * Major\ Axis^2} \quad (2)$$

2.5. Biocompatibility assay

An MTT cell proliferation assay kit (Ab211091, Abcam, UK) was used to evaluate cell viability at the 2D MOF interfaces. To define the cell culture areas, MOFs substrates were attached to a customized, bottom-less 48-well plate (Greiner 677,980, Austria) with 1.0 cm^2/well growth area. Then, PC12 cells were detached from the petri dishes and seeded to the PLL-coated MOF samples with a density of 71.5 k/cm^2. The cell number was counted by a Countess 3 Cell Counter set-up from ThermoFisher Scientific (US). After 24-h of cell culture, the medium was replaced by adding 150 μL of serum-free media and 150 μL MTT reagent into each sample well. As background control, 150 μL of serum-free media and 150 μL MTT reagent were added into a blank well. Plates were incubated at 37 °C in a 5% CO_2 incubator for 3 h. After incubation, 450 μL MTT solvent was added into each well (including the control well), followed with another incubation at 37 °C for 15 min in dark. Then MTT contained sample medium was transferred to a new 96-well plate for absorbance reading. Ending absorbance at OD = 590 nm was recorded by microplate reader (Molecular Device, SpectraMax® iD5). The acquired data was normalized to either bare glass (for MOFs on glass) or bare gold (for MOFs on Au) substrates separately and presented in percent (%).

2.6. Cellular reactive oxygen species (ROS) evaluation

The DCFDA/H2DCFDA - Cellular ROS Assay kit (ab 113,851, Abcam, UK) was used to assess the amount of reactive oxygen species in live PC-12 cells. Briefly, small vials from the assay kit were centrifuged at low speed prior to opening. To prepare a 1*x* buffer ready for usage, the 10*x* buffer from the kit was diluted with DI water. The 1*x* buffer was kept inside fridge and equilibrated to 37 °C before usage. To prepare a working DCFDA solution, 20 mM DCFDA was freshly diluted to a 20 μM final concentration with the 1*x* buffer.

To define the cell culture areas, MOFs substrates were attached to customized bottom-less 48-well plates (Greiner 677,980, Austria) with a final 1.0 cm^2/well growth area. Cells were seeded into each well with a final density at 71.5 k/cm^2. The medium was removed after 24-h cell incubation and rinsed with the 1*x* buffer (300 μL/well). Then cells were stained with 300 μL/well of the DCFDA working solution. Thereafter, the cells were incubated with DCFDA working solution for 1 h at 37 °C. Then the DCFDA solution was replaced in a 1*x* buffer (300 μL/well). The plates were measured immediately using a microplate reader (Molecular Device, SpectraMax® iD5) at Ex/Em = 485/535 nm in the end point mode in presence of cells and medium. The acquired data was normalized to either bare glass (for MOFs on glass) or bare gold (for MOFs on Au) control substrates separately and the data is presented in percentage (%) values.

2.7. Sample preparation for electron microscopy and focused ion beam milling

The samples were prepared following the ultra-thin plasticization procedure (Santoro et al., 2017; Wrobel et al., 2008). The biological samples were initially treated with 4% v/v paraformaldehyde dissolved in Milli-Q water, for chemical fixation. This was followed by an overnight incubation at 4 °C in 2.5% v/v glutaraldehyde (Electron Microscopy Science) diluted in 0.1 M cacodylate buffer. Subsequently, samples were rinsed with a 0.1 M cacodylate solution while being kept on ice throughout these procedures. Next, the buffer solution was substituted with a 20 mM glycine solution, prepared with 0.1 M sodium cacodylate, and the samples were allowed to incubate for 20 min. Following this, the specimens were placed in a solution containing 4% v/v aqueous osmium tetroxide (Electron Microscopy Science) and 2% potassium ferrocyanide (Electron Microscopy Science) for a duration of 1 h at 4 °C, while being shielded from direct light. Subsequently, the samples were subjected to three washes with a 0.1 M cacodylate buffer solution. To conclude, a final incubation was carried out using a 2% v/v aqueous osmium tetroxide solution (Electron Microscopy Science) at room temperature for 30 min. The specimens were meticulously rinsed with DI water at room temperature and then immersed in a 1% filtered thiocarbohydrazide (TCH), (Electron Microscopy Science, USA solution in DI water for 20 min at room temperature. Afterwards, the samples underwent three rounds of rinsing with DI water. Subsequently, they were immersed overnight at 4 °C in an En bloc staining solution consisting of 4% v/v uranyl acetate. After this, the samples were subjected to additional three rinses of DI water and then placed in a 0.15% v/v tannic acid solution (by Sigma Aldrich) for a brief 3-min incubation at 4 °C. Dehydration was carried out through a sequence of ethanol dilutions (30% v/v, 50% v/v, 75% v/v, 2 × 95% v/v, and 100% v/v ethanol in water), each step lasting for 10 min at 4 °C. Additionally, 100% ethanol was replaced twice at room temperature. Finally, the samples were gradually embedded in resin (comprising 25 mL of NSA, 8 mL D.E.R. 736, 10 mL of ERL 4221, and 301 μL of DMAE, obtained from Electron Microscopy Science) using varying ethanol-to-resin ratios. The initial embedding involved a mixture of ethanol and resin with a 1:3 ratio, and the sample remained embedded for 2 h. Subsequently, the second ratio used was 1:2, and this embedding step also lasted for 2 h. Finally, the last embedding was carried out using pure resin and was left in place overnight and throughout the day. Afterwards, the specimens were positioned vertically for 2 h and then polymerized at 70 °C for 24 h. To prepare the samples for electron microscopy imaging, they were affixed to aluminium stubs with a diameter of 3.2 mm using silver conductive paste (RS Pro, country) and coated with a 15 nm thick layer of gold before imaging.

2.8. Focused ion beam - scanning electron microscopy (SEM-FIB)

The specimens were loaded inside the dual-beam vacuum chamber (Thermo Fischer, Helios NanoLab 600i and 650). Firstly, the region of interest (ROI) was detected and then the stage was tilted at 52°. Afterwards, one deposition layer was performed by ion beam deposition (0.3 μm thickness of platinum, with a beam current of 0.43 nA and 30 kV acceleration voltage). Cross sections were performed by first trenching out the material via an ion beam (cutting thickness: 5 μm; current: 0.79 nA; acceleration voltage: 30 kV). The ion beam was then used to polish the interface (current: 0.23–0.43 nA; acceleration voltage: 30 kV). Scanning electron micrographs were acquired in back scattering mode at high resolution with a dwell time of 20 μs and an electron beam with acceleration voltage of 3 kV and a beam current of 0.17 nA.

2.9. Structural and morphological characterizations

Optical images of the Au substrate and the 2D Fe-MOF thin films on Au substrate were captured by a Confocal Laser Microscope (Keyence, VK-X200). Grazing incidence X-ray diffraction (GIXRD) was conducted on an X'Pert pro (PANalytical, CuKα λ = 1.5406 Å) from 3° to 50° with a step of 0.1° to evaluate the crystallinity and eventual impurities in the 2D Fe-MOF on Au substrates. The thickness and topographic evaluations of the 2D Fe-MOF were carried out by Atomic Force Microscopy (AFM, NX20, Park systems) and Scanning Electron Microscopy (SEM, Zeiss) and energy dispersive X-ray spectroscopy (EDAX) techniques. Water contact angles were characterized using a dynamic contact angle measurement set-up (DataPhysics OCA15EC).

2.10. Electrochemical impedance spectroscopy

EIS characterizations (two-electrode configuration using Platinum wire as a counter electrode) of 2D Fe-MOF modified electrodes (0.3 × 0.2 mm^2 x 12 = 0.72 mm^2) were done using a potentiostat (Pico Emstat from Palmsens) and the spectra were recorded in the frequency ranges from 5 Hz to 200 kHz, while a small AC potential of 50 mV was applied. Initially, long-term EIS spectra were recorded every 5 min for 24 h to

evaluate the electrochemical stability of the 2D Fe-MOF in cell culture medium without PC-12 cells. Then, the PC-12 cells were seeded with a density of 200 k cells/cm^2, and immediately, long-term EIS spectra were collected with the same parameters for 24 h.

3. Results and discussion

As illustrated in Fig. 1 and described in **Section 2.1**, 2D Fe-MOF were synthesized on Au substrates functionalized with hydroxyl groups by carrying out twenty LbL-LPE cycles using the automated dip coater. These samples are denoted as Fe-MOF-20c. Initially, the successful growth of homogeneous Fe-MOF thin films was observed by confocal laser microscopy. As shown in Fig. 2a, regions of Au substrate and Fe-MOF are clearly visible. In order to characterize the thickness of the LPE grown MOFs, a photolithography process was developed to pattern the MOFs on arbitrary substrates. The developed protocol to micro-pattern 2D Fe-MOF is described in Fig. S2 in the **SI**. Once micro-patterned, the thickness of Fe-MOF-20c was characterized by AFM. As can be seen in Fig. 2b, the thickness was about 20 nm, forming an ultra-thin functional 2D interface on Au substrates, which can also be used as an electrode for the EIS measurements. A low surface roughness value of R_a = 3.9 nm demonstrates the smoothness of 2D Fe-MOF surface (Fig. 2c). As expected for the LPE grown 2D MOFs, the resulting surface roughness after growth is much higher in comparison to the Au electrode with an average roughness value R_a = ~1.0 nm and a MUD functionalized Au electrode measured at R_a = ~1.0 nm (shown in Figs. S3 and S4). The corresponding amplitude image shows a consistent tip-deflection and suggests a high homogeneity of the 2D Fe-MOF coating on the Au electrodes (Fig. 2d). Additionally, the successful growth of the 2D Fe-MOF on Au is identified by comparative analysis of water contact angle measurements on bare Au substrates, MUD functionalized Au substrates, and Fe-MOF-20c on Au (Fig. 2e–g). The significant decrease of the contact angle from 84.8° to 55.4° indicates a successful introduction of hydroxyl groups on Au substrates. Then, the obvious increase of the contact angle from 55.4° to 61.5° implies the growth of Fe-MOF on the functionalized Au substrate. Furthermore, the contact angle (61.5°) for Fe-MOF-20c suggests a hydrophilic character of these novel 2D interfaces with wettability behaviour favourable for live cells to attach and spread due to the potential interactions between Fe-MOF and membrane proteins (Cui et al., 2020).

The crystallographic structure of the grown 2D Fe-MOF was evaluated using GIXRD measurements, as shown in Fig. 2h two sharp peaks at 38.6° and 44.8° are observable, which can be ascribed to the Au substrate. The two weaker angel peaks are at 8.94° and 10.02° and a broad peak seen at ~12.5° is contributed by the Fe-MOF, indicating a relatively low crystallinity characteristic of the developed 2D films (Huang et al., 2022). From the GIXRD measurements, no elemental impurities were observed either foreign or from the precursors used in the growth process. The SEM scan image shown in Fig. 2i again demonstrates the homogeneous growth of a typical 2D Fe-MOF layer on the Au substrates. Herein, from an EDAX spectrum as shown in the image inset, C, O, N, and Fe elements were recognized, confirming the formation of coordination frameworks between Fe^{3+} ions and BDC-NH_2 linkers but with a short-range order.

After confirming the stable and reliable growth of MOF thin films, we characterized the biocompatibility of 2D MOF layers. For this, samples of two 2D MOF thin films (Fe-MOF and Ni-MOF) were prepared on glass and gold substrates and were evaluated with PC-12 cells after 24-h incubation as shown in Fig. 3. The viability assessed from the MTT assays of PC-12 was normalized to bare glass (for MOFs on glass) and bare gold (for MOFs on Au) individually to compare the influence of the MOFs on the different substrates. An average increase in PC-12 viability after 24 h was observed for both Fe-MOF/glass (108.3 ± 42.8 %) and Ni-MOF/glass (123.1 ± 42.9 %) substrates, as compared to that for the bare glass (95.4 ± 24.2 %) substrates. This metabolic viability result proved the biocompatibility of 2D MOF interfaces realized on glass substrates. For Fe-MOF/Au (69.9 ± 18.9 %) substrates, however, a lower viability was noticed in comparison to that of the bare Au substrate (100.0 ± 15.0 %) and for Ni-MOF/Au (107.7 ± 28.3 %) with significant statistical difference, as illustrated in Fig. 3a. The varying viability results on Au substrates suggested the potential surface interaction between Fe-MOF and Au, and potentially provide opportunities to regulate the bio-activities at such 2D MOF layers.

To further understand the potential of Fe- and Ni-based MOFs in regulating cellular activity, ROS generation of PC-12 was measured after 24 h incubation to evaluate the cellular oxidative stress. The corresponding data-sets are presented in percent (%) after normalization to bare glass (for MOFs on glass) and bare gold (for MOFs on Au) as shown

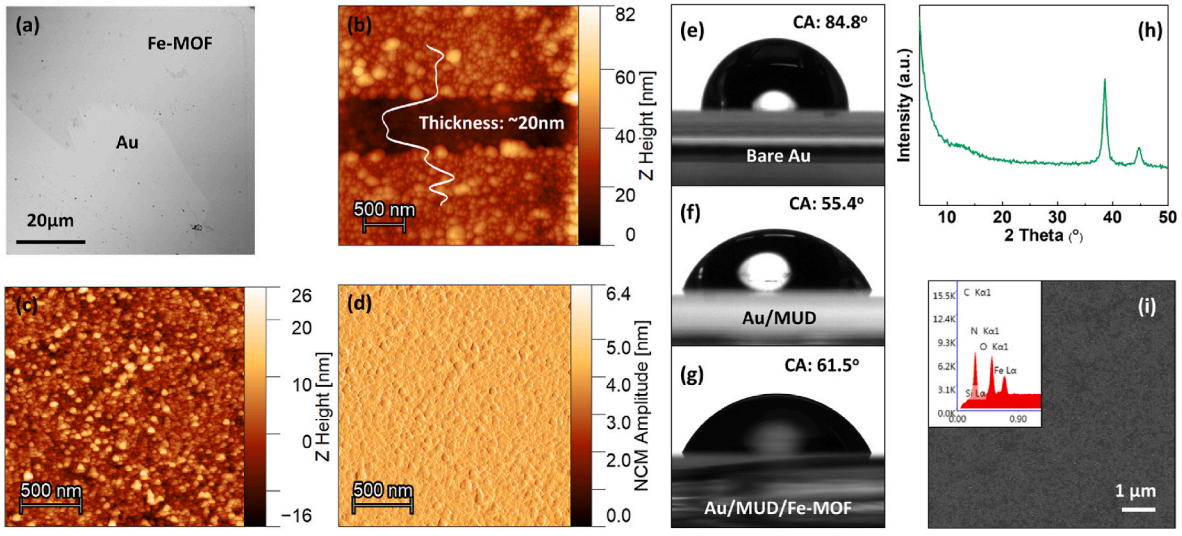

Fig. 2. Surface and material characterization of a typical 2D MOF sample. (a) A zoomed in optical image of 2D Fe-MOF on an Au chip shows the clear borders of the LbL-LPE growth edges. (b) AFM topographic scan of a 2D Fe-MOF layer through a nanoscale trench revealing the height profile of the growth. (c, d) Scans representing height and amplitude signal from the AFM for a typical MOF region. (e–f) Images showing water contact angle at bare Au, MUD-functionalized Au, and 2D Fe-MOF interfaces (h) Grazing incidence XRD pattern of Fe-MOF on an Au substrate indicates a crystal lattice typical of such MOF based porous crystalline 2D material systems. (i) SEM image of the 2D Fe-MOF show a consistent topography and the corresponding EDAX spectrum indicates the presence of C, N, O, and Fe as elemental components.

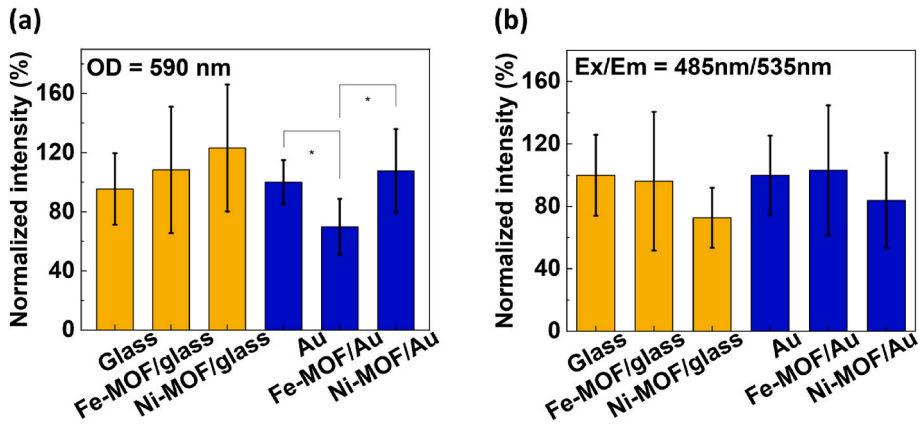

Fig. 3. Biocompatibility characterizations of LbL-LPE grown 2D MOFs with the PC-12 cell line. (a) Fluorescence absorbance recorded from the PC-12 cell cultures when performing MTT cell proliferation assays on 2D MOFs grown on glass and gold chips, together with controls. Higher normalized intensities indicate better cell viability. (b) Evaluation of cellular reactive oxygen species (ROS) after 24 h of PC-12 cell culture on the different 2D MOF samples with relevant control samples. Higher normalized intensity values indicate a high oxidative stress. (For interpretation of the references to colour in this figure legend, the reader is referred to the Web version of this article.)

in Fig. 3b, where higher values indicate higher ROS levels. Here, similar ROS generation was recorded in bare glass (100.0 ± 25.9 %) and Fe-MOF/glass (96.2 ± 44.5 %), while lower ROS was observed in Ni-MOF/glass (72.2 ± 19.2 %). Comparably, Fe-MOF/Au (103.1 ± 41.7 %) yielded similar ROS level of PC-12 with bare Au (100.0 ± 25.4 %), while a ROS reduction appeared in Ni-MOF/Au (83.8 ± 30.5 %). These measurement results indicated the ROS reduction ability of Ni-MOFs, on glass as well as on Au substrates, in agreement with the biocompatibility evaluation. Considering the redox behaviour of Fe and Ni as transition metals, these results supported the ability of Fe- and Ni-chelated MOFs in regulating oxidative stress and therefore improving cell viability, giving opportunity towards redox active biosensors (Boschker et al., 2021; Gao et al., 2020).

Morphological analyses were carried out after immunostaining F-actin (red), paxillin (green) and nuclei (blue), as shown in Fig. 4a–e. When comparing MOF layers to those of standard glass substrates, PC-12 cells demonstrated smaller aspect ratios (AR) on both Fe- and Ni-MOFs and a bigger cell coverage area on Ni-MOF/Au. The smaller AR can also be clearly seen from the roundness parameter also, which is related to AR, as presented in Fig. S5. After further comparison between Fe-MOF and Ni-MOF, no difference was found in AR and roundness. Overall, the cells were more elongated on Ni-MOF/Au with lower circularity value compared to Fe-MOF/glass surfaces. In terms of the coverage area comparison for both 2D MOFs, Ni-MOF/Au interfaces

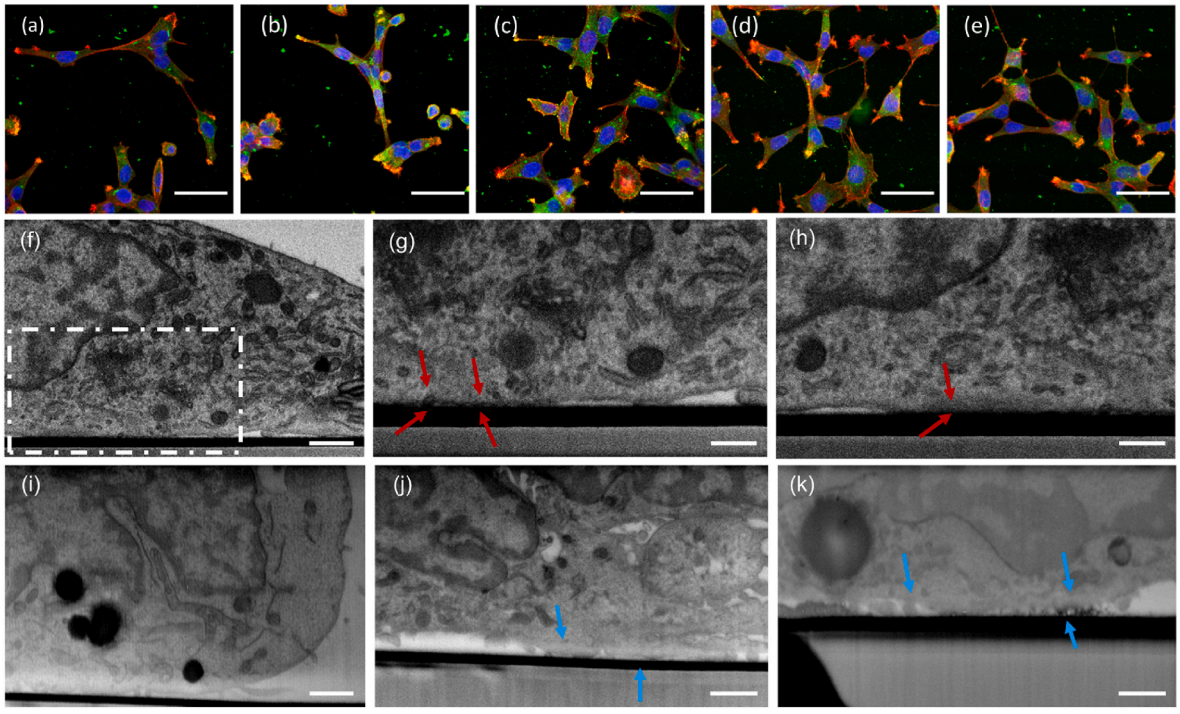

Fig. 4. Morphological analyses of PC-12 cells on LbL-LPE grown 2D MOF samples. Exemplary fluorescence microscopy images of PC-12 cells after immunostaining on (a) cover glass, (b) Ni-MOF/glass, (c) Fe-MOF/glass, (d) Ni-MOF/Au, (e) Fe-MOF/Au. Scale bar: 50 μm. Morphology was analysed and statistical data are presented in Fig. S5 of the SI. Actin cytoskeleton (red), focal adhesion (green), nuclei (blue). SEM-FIB analysis of PC-12 cell adhesion on different surfaces: (f–h) Ni-MOF/Au substrate, (i–k) Fe-MOF/Au substrate. The black line indicates the original electrode surfaces and arrows point towards the focal adhesion sites. Scale bar is 500 nm. (For interpretation of the references to colour in this figure legend, the reader is referred to the Web version of this article.)

yielded a higher cell coverage area and perimeter in comparison to Fe-MOF/Au and other substrates (Fig. S5). This is further evidence that Fe-MOF and Ni-MOF are beneficial in regulating the cytoskeleton structures compared to non-functionalized bare substrates, which could also be a result of the lower ROS concentrations at these cell-chip interface.

The contact area between PC-12 cells and the imposed topography was visualized by means of SEM and in situ cross-section imaging by focused ion beam milling. On both Ni-MOF/Au and Fe-MOF/Au, the plasma membrane follows the metal profiles (Fig. 4f–k). Micrographs displaying the interaction between PC-12 cells and Ni-MOF/Au (Fig. 4f–h) suggested that the cells are actively interacting with the imposed magnetic metal topography (red arrows). In turn, in Fig. 4i–k showing PC-12 cells on Fe-MOF/Au the high magnetic property of Fe leads to the formation of the white halo and detaching phases (blue arrows). FIB-SEM micrographs also show that as cells explore the substrate underneath, importantly the cross sections reveal the presence of the membrane invagination (red arrows). The porous nature of the MOF lattice and the topography is expected to allow an altered but favourable interaction for cell membrane influencing the cell adhesion, proliferation, and differentiation resulting in higher cell viability. Such favourable interactions make MOFs as desirable active substrates for stimulation and recordings from biological systems. Here, ECIS serves as an ideal non-invasive technique for the study of cell-substrate interactions, cell-behaviour against new materials and to optimize electrochemical parameters that are fundamental to the development of future bioelectronics platforms.

Prior to the study of cell-substrate interaction by the ECIS technique, the long-term electrochemical stability of Fe-MOF thin film in cell culture medium was evaluated by conducting EIS measurements with a small AC potential of 50 mV from 5 Hz to 200 kHz. As shown in Fig. S6, significant decrease in impedance amplitude was observed after 24 h incubation, most probably due to ion intercalation into the porous Fe-MOF matrix. Besides, the change in phase also indicates the influence of the culture medium within the Fe-MOF matrix. Furthermore, the impedance amplitude of the Fe-MOF/Au substrate was monitored and analysed at a fixed frequency of 200 kHz for 24 h, as shown in Fig. S7. The impedance amplitude deceased dramatically and rose then steadily after 4 h. After 16 h a quasi-equilibrium state was reached at the Fe-MOF interface over 20 h. This stable response is crucial for the ECIS measurements with cells to exclude the contribution to the change of impedance from the Fe-MOF itself.

The EIS characterizations of the cell cultures involved seeding of PC-12 cells onto the 2D Fe-MOF samples realized on Au electrodes, where a significant increase in impedance was observed at the frequencies around 10 kHz after 24 h, while no apparent change at lower frequencies (<1 kHz) can be seen (Fig. 5a). Besides, the change of phase in the frequency range for 24 h is shown in Fig. 5b, implying the successful attachments of cells. To find the optimal frequency to monitor the behaviour of the cells (e., g. Attachment, spearing, and proliferation) on Fe-MOF interface, the impedance was normalized according to: $Z_{w/\ cells}/Z_{w/o\ cells}$ (w/= with, w/o = without). As shown in Fig. 5c, the impedance amplitude shows the maximum change at a frequency of 12.6 kHz. Then, the PC-12 cell growth and spreading were monitored and studied at this fixed frequency for 24 h. A quick increase in impedance amplitude was observed after cell seeding within 4 h, shown in Fig. 5d. A slight decrease of the impedance amplitude was observed from 4 to 8 h, which is known as response to cell spreading on the Fe-MOF interface. Subsequently, PC-12 cells started to grow and proliferate in the next 10 h, which resulted in the continue increase in impedance due to the rising coverage onto the Fe-MOF/Au electrode with cells (Szulcek et al., 2014). As indicated in Fig. 5d–a confluent cell layer was formed after 20 h due to the saturation of impedance from 20 to 24 h, which was also confirmed by an optical microscopy image captured after 24 h (Fig. S8). Finally, to understand how attached cells influence the Fe-MOF layer, electrically equivalent circuits were simulated as shown in Fig. 5e and f before and after cell attachment. Herein, there are three components to model the contribution of the PC-12 cells, $R_{Junction}$, R_{Cell}, and $C_{Membrane}$, due to the formation of a confluent layer. The fitted curves and parameters before and after cell attachment are shown in Fig. S9, Fig. S10 and Table 1, respectively. These experimental and modelling results are in a good agreement, thus validating the electrical model.

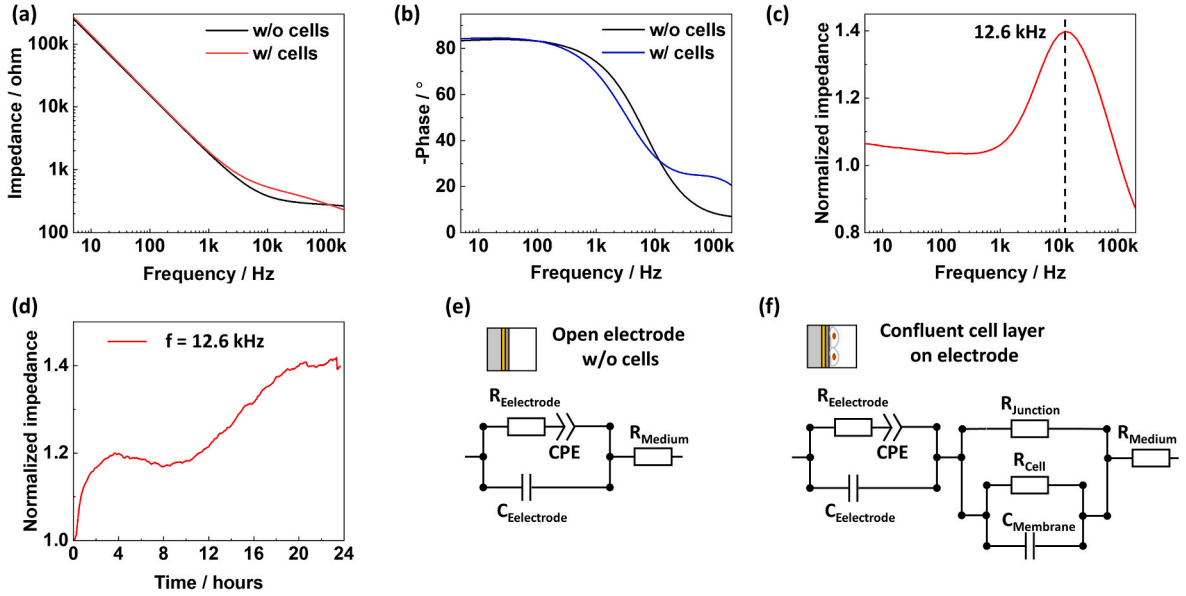

Fig. 5. Long-term EIS characterization of the PC-12 cell culture on Fe-MOF modified gold electrodes. (a) Impedance spectrum of a typical Fe-MOF modified gold electrode w/o cell (black curve) compared with impedance spectrum (red curve) after 24 h of cell-culture. (b) Characteristic phase change recorded w/o (black curve) and w/the cells (blue curve) after 24 h of cell culture. (c) Normalized impedance spectral response w/o and w/cells. (d) Real-time EIS response of the 2D Fe-MOF modified electrode over 24 h after the seeding of PC-12 cells recorded at 12.6 kHz inside an incubator. (e, f) Illustrations show the equivalent electrical circuits for the EIS measurement set-up with and w/o cells (Chen et al., 2011). (For interpretation of the references to colour in this figure legend, the reader is referred to the Web version of this article.)

Table 1
Summary of the electrical parameters derived from the EIS measurements using the equivalent circuit as shown in Fig. 5. Corresponding fits to the data are shown in the SI in Fig. S9 and Fig. S10.

		w/o cells	w/ cells
R_{Medium}/Ω		252.6	192.4
$R_{Electrode}/\Omega$		88.87	232.9
$C_{Electrode}$/nF		23.68	9.847
CPE	Q/μT	0.141	0.137
	n	0.913	0.936
$R_{Junction}/\Omega$		NA	209.7
R_{Cell}/Ω		NA	310.4
$C_{Membrane}$/nF		NA	129.4

4. Conclusions

Two-dimensional layers based on Fe-MOF and Ni-MOF were successfully realized onto glass and Au substrates. In order to characterize their biocompatibility, a metabolic and a ROS assay were done with the PC-12 neuroblastoma cell line, which confirmed that cells survive and proliferate, rendering MOFs as a new class of porous, crystalline and electrically tunable 2D materials. They present novel opportunties to develop bioelectronic and biosensor applications. The cell-attachment, spreading and proliferation steps were studied via employing the ECIS technique using Fe-MOF/Au samples, which in turn could monitor different stages of cell spreading and proliferation in realtime. To the best of our knowledge, this is the first demonstration of utilizing 2D MOF interfaces to study the cell-substrate interactions using the ECIS technique. Development of such surface coatings based on MOFs could aid to study the dynamics of living systems in detail to support the emerging usage of MOFs such as biological scaffolds and implants (Shen et al., 2022; Wu et al., 2022). Further, routine integration of novel 2D MOFs as demostrated in this work, opens up the opportunity to carry out fundamental studies of underlying effects that regulate the biological activity and are expected to be advantageous in designing future solutions for stimulation and recording of biological signals.

CRediT authorship contribution statement

Huijie Jiang: Writing – original draft, Visualization, Validation, Methodology, Investigation, Formal analysis, Data curation. **Ziyu Gao:** Writing – original draft, Visualization, Validation, Methodology. **Claudia Lubrano:** Visualization, Methodology, Formal analysis, Data curation. **Claudia Latte Bovio:** Visualization, Investigation, Formal analysis, Data curation. **Henning Bommes:** Visualization, Investigation, Data curation. **Andrea Kauth:** Validation, Formal analysis, Data curation. **Lea Baumann:** Methodology, Data curation. **Bo Cheng:** Visualization, Software, Resources, Methodology. **Divagar Murugan:** Visualization, Methodology, Data curation. **Joachim Knoch:** Resources. **Rainer Waser:** Resources. **Sven Ingebrandt:** Writing – review & editing, Supervision, Resources, Methodology. **Francesca Santoro:** Writing – review & editing, Supervision, Methodology, Funding acquisition, Data curation. **Vivek Pachauri:** Writing – review & editing, Writing – original draft, Supervision, Resources, Project administration, Methodology, Funding acquisition, Formal analysis, Data curation, Conceptualization.

Declaration of competing interest

The authors declare that they have no known competing financial interests or personal relationships that could have appeared to influence the work reported in this paper.

Data availability

Data will be made available on request.

Acknowledgements

The research work presentaed in this manuscript was supported by the Deutsche Forschungsgemeinschaft (DFG) projects MOFSens (no. 445865083) and project InnoRetvision (no. 424556709/GRK2610). Huijie Jiang also acknowldges support from the Chinese Scholarship Council for his fellowship. Francesca Santoro and Ziyu Gao acknowledge funding from the European Research Council (ERC) under the European Union's Horizon 2020 research and innovation programme (BRAIN-ACT, Grant agreement No. 949478). Microfabrication was carried out in the Central Laboratory for Micro- and Nanotechnology (CMNT) at RWTH Aachen University. Technical support by CMNT staff is gratefully acknowledged. In addition, we thank Jochen Heiss, Dorothee Breuer, Eva-Janina Sekula and Lisa Hertje (all IWE1, RWTH Aachen University) for their help during microfabrication.

Appendix A. Supplementary data

Supplementary data to this article can be found online at https://doi.org/10.1016/j.biosx.2024.100487.

References

Boschker, H.T.S., Cook, P.L.M., Polerecky, L., Eachambadi, R.T., Lozano, H., Hidalgo-Martinez, S., Khalenkow, D., Spampinato, V., Claes, N., Kundu, P., Wang, D., Bals, S., Sand, K.K., Cavezza, F., Hauffman, T., Bjerg, J.T., Skirtach, A.G., Kochan, K., McKee, M., Wood, B., Bedolla, D., Gianoncelli, A., Geerlings, N.M.J., Van Gerven, N., Remaut, H., Geelhoed, J.S., Millan-Solsona, R., Fumagalli, L., Nielsen, L.P., Franquet, A., Manca, J.V., Gomila, G., Meysman, F.J.R., 2021. Efficient long-range conduction in cable bacteria through nickel protein wires. Nat. Commun. 12 (1), 3996.
Chen, C.-C., Lin, S.-Y., Sheu, J.-T., 2011. Using impedance biosensors to distinguish the PC12 cells adhesion and differentiation. In: 2011 6th IEEE International Conference on Nano/Micro Engineered and Molecular Systems, pp. 813–816.
Chen, S., Surendran, A., Wu, X., Lee, S.Y., Stephen, M., Leong, W.L., 2020. Recent technological advances in fabrication and application of organic electrochemical transistors. Adv Mater Technol 5 (12), 2000523.
Cui, H., Wang, W., Shi, L., Song, W., Wang, S., 2020. Superwettable surface engineering in controlling cell adhesion for emerging bioapplications. Small Methods 4 (12).
Cui, Y., Li, B., He, H., Zhou, W., Chen, B., Qian, G., 2016. Metal-organic frameworks as platforms for functional materials. Acc. Chem. Res. 49 (3), 483–493.
Dhanapala, B.D., Maglich, D.L., Anderson, M.E., 2023. Impact of surface functionalization and deposition method on Cu-bdc surMOF formation, morphology, crystallinity, and stability. Langmuir 39 (34), 12196–12205.
Diring, S., Carne-Sanchez, A., Zhang, J., Ikemura, S., Kim, C., Inaba, H., Kitagawa, S., Furukawa, S., 2017. Light responsive metal-organic frameworks as controllable CO-releasing cell culture substrates. Chem. Sci. 8 (3), 2381–2386.
Ejeian, F., Razmjou, A., Nasr-Esfahani, M.H., Mohammad, M., Karamali, F., Ebrahimi Warkiani, M., Asadnia, M., Chen, V., 2020. ZIF-8 modified polypropylene membrane: a biomimetic cell culture platform with a view to the improvement of guided bone regeneration. Int. J. Nanomed. 15, 10029–10043.
Ermis, M., Antmen, E., Hasirci, V., 2018. Micro and Nanofabrication methods to control cell-substrate interactions and cell behavior: a review from the tissue engineering perspective. Bioact. Mater. 3 (3), 355–369.
Furukawa, H., Cordova, K.E., O'Keeffe, M., Yaghi, O.M., 2013. The chemistry and applications of metal-organic frameworks. Science 341 (6149), 1230444.
Gao, Z., Carames-Mendez, P., Xia, D., Pask, C.M., McGowan, P.C., Bingham, P.A., Scrimshire, A., Tronci, G., Thornton, P.D., 2020. The facile and additive-free synthesis of a cell-friendly iron(iii)-glutathione complex. Dalton Trans. 49 (30), 10574–10579.
Ghafar-Zadeh, E., Sawan, M., Chodavarapu, V.P., Hosseini-Nia, T., 2010. Bacteria growth monitoring through a differential CMOS capacitive sensor. IEEE Trans Biomed Circuits Syst 4 (4), 232–238.
Hanke, M., Arslan, H.K., Bauer, S., Zybaylo, O., Christophis, C., Gliemann, H., Rosenhahn, A., Wöll, C., 2012. The biocompatibility of metal–organic framework coatings: an investigation on the stability of SURMOFs with regard to water and selected cell culture media. Langmuir 28 (17), 6877–6884.
Hedayatipour, A., Aslanzadeh, S., McFarlane, N., 2019. CMOS based whole cell impedance sensing: challenges and future outlook. Biosens. Bioelectron. 143, 111600.
Hempel, F., Law, J.K.Y., Nguyen, T.C., Lanche, R., Susloparova, A., Vu, X.T., Ingebrandt, S., 2021. PEDOT:PSS organic electrochemical transistors for electrical cell-substrate impedance sensing down to single cells. Biosens. Bioelectron. 180, 113101.
Hong, J., Kandasamy, K., Marimuthu, M., Choi, C.S., Kim, S., 2011. Electrical cell-substrate impedance sensing as a non-invasive tool for cancer cell study. Analyst 136 (2), 237–245.

Horcajada, P., Gref, R., Baati, T., Allan, P.K., Maurin, G., Couvreur, P., Ferey, G., Morris, R.E., Serre, C., 2012. Metal-organic frameworks in biomedicine. Chem. Rev. 112 (2), 1232–1268.
Huang, P., Yao, L., Chang, Q., Sha, Y., Jiang, G., Zhang, S., Li, Z., 2022. Room-temperature preparation of highly efficient NH(2)-MIL-101(Fe) catalyst: the important role of -NH(2) in accelerating Fe(III)/Fe(II) cycling. Chemosphere 291 (Pt 3), 133026.
Katayama, T., Tanaka, S., Tsuruoka, T., Nagahama, K., 2022. Two-dimensional metal-organic framework-based cellular scaffolds with high protein adsorption, retention, and replenishment capabilities. ACS Appl. Mater. Interfaces 14 (30), 34443–34454.
Kavand, H., Nasiri, R., Herland, A., 2022. Advanced materials and sensors for microphysiological systems: focus on electronic and electrooptical interfaces. Adv. Mater. 34 (17), e2107876.
Kreno, L.E., Leong, K., Farha, O.K., Allendorf, M., Van Duyne, R.P., Hupp, J.T., 2012. Metal-organic framework materials as chemical sensors. Chem. Rev. 112 (2), 1105–1125.
Kuppler, R.J., Timmons, D.J., Fang, Q.-R., Li, J.-R., Makal, T.A., Young, M.D., Yuan, D., Zhao, D., Zhuang, W., Zhou, H.-C., 2009. Potential applications of metal-organic frameworks. Coord. Chem. Rev. 253 (23–24), 3042–3066.
Li, Y., Cui, B., Zhang, S., Li, B., Li, J., Liu, S., Zhao, Q., 2022. Ion-selective organic electrochemical transistors: recent progress and challenges. Small 18 (19), e2107413.
Liao, P.-Q., Shen, J.-Q., Zhang, J.-P., 2018. Metal–organic frameworks for electrocatalysis. Coord. Chem. Rev. 373, 22–48.
Lin, Q., Cheon, J.h., Gong, B.D., Park, Y.J., Min, H.s., Kang, D.w., Kim, L., Suh, J.S., 2006. Capacitive measurements for a novel ECIS (electrolyte–carbon nanotubes–insulator–semiconductor) structure. Semicond. Sci. Technol. 21 (5), 686–690.
Liu, F., Nordin, A.N., Li, F., Voiculescu, I., 2014. A lab-on-chip cell-based biosensor for label-free sensing of water toxicants. Lab Chip 14 (7), 1270–1280.
Long, J.R., Yaghi, O.M., 2009. The pervasive chemistry of metal-organic frameworks. Chem. Soc. Rev. 38 (5), 1213–1214.
Marks, A., Griggs, S., Gasparini, N., Moser, M., 2022. Organic electrochemical transistors: an emerging technology for biosensing. Adv. Mater. Interfac. 9 (6), 2102039.
McKinlay, A.C., Morris, R.E., Horcajada, P., Ferey, G., Gref, R., Couvreur, P., Serre, C., 2010. BioMOFs: metal-organic frameworks for biological and medical applications. Angew Chem. Int. Ed. Engl. 49 (36), 6260–6266.
Miller, J.G., 1973. Living systems. I. The nature of living systems. Quad. Criminol. Clin. 48 (1), 63–91.
Nawaz, A., Liu, Q., Leong, W.L., Fairfull-Smith, K.E., Sonar, P., 2021. Organic electrochemical transistors for in vivo bioelectronics. Adv. Mater. 33 (49), e2101874.
Pitsalidis, C., Pappa, A.M., Boys, A.J., Fu, Y., Moysidou, C.M., van Niekerk, D., Saez, J., Savva, A., Iandolo, D., Owens, R.M., 2022. Organic bioelectronics for in vitro systems. Chem. Rev. 122 (4), 4700–4790.
Rajendran, A.K., Sankar, D., Amirthalingam, S., Kim, H.D., Rangasamy, J., Hwang, N.S., 2023. Trends in mechanobiology guided tissue engineering and tools to study cell-substrate interactions: a brief review. Biomater. Res. 27 (1), 55.
Rossetti, N., Hagler, J.E., Kateb, P., Cicoira, F., 2021. Neural and electromyography PEDOT electrodes for invasive stimulation and recording. J. Mater. Chem. C 9 (23), 7243–7263.
Santoro, F., Zhao, W., Joubert, L.M., Duan, L., Schnitker, J., van de Burgt, Y., Lou, H.Y., Liu, B., Salleo, A., Cui, L., Cui, Y., Cui, B., 2017. Revealing the cell-material interface with nanometer resolution by focused ion beam/scanning electron microscopy. ACS Nano 11 (8), 8320–8328.
Semrau, A.L., Zhou, Z., Mukherjee, S., Tu, M., Li, W., Fischer, R.A., 2021. Surface-mounted metal-organic frameworks: past, present, and future perspectives. Langmuir 37 (23), 6847–6863.
Shen, X., Hii Ru Yie, K., Wu, X., Zhou, Z., Sun, A., Al-bishari, A.M., Fang, K., Al-Baadani, M.A., Deng, Z., Ma, P., Liu, J., 2022. Improvement of aqueous stability and anti-osteoporosis properties of Zn-MOF coatings on titanium implants by hydrophobic raloxifene. Chem. Eng. J. 430.
Sniadecki, N.J., Desai, R.A., Ruiz, S.A., Chen, C.S., 2006. Nanotechnology for cell-substrate interactions. Ann. Biomed. Eng. 34 (1), 59–74.
Szulcek, R., Bogaard, H.J., van Nieuw Amerongen, G.P., 2014. Electric cell-substrate impedance sensing for the quantification of endothelial proliferation, barrier function, and motility. J. Vis. Exp. 85.
Vandrovcová, M., Bacáková, L., 2011. Adhesion, growth and differentiation of osteoblasts on surface-modified materials developed for bone implants. Physiol. Res. 60 (3), 403–417.
Vinzons, L.U., Gupta, A.K., Lai, T.-Y., Lin, S.-P., 2022. Interpretation of biosensing technology in cell-coupled silicon nanowire transistors via impedance spectra. Mater. Lett. 308.
Vodyashkin, A.A., Sergorodceva, A.V., Kezimana, P., Stanishevskiy, Y.M., 2023. Metal-organic framework (MOF)-A universal material for biomedicine. Int. J. Mol. Sci. 24 (9), 7819.
Wang, L., Wang, H., Wang, L., Mitchelson, K., Yu, Z., Cheng, J., 2008. Analysis of the sensitivity and frequency characteristics of coplanar electrical cell-substrate impedance sensors. Biosens. Bioelectron. 24 (1), 14–21.
Wegener, J., Keese, C.R., Giaever, I., 2000. Electric cell-substrate impedance sensing (ECIS) as a noninvasive means to monitor the kinetics of cell spreading to artificial surfaces. Exp. Cell Res. 259 (1), 158–166.
Wrobel, G., Holler, M., Ingebrandt, S., Dieluweit, S., Sommerhage, F., Bochem, H.P., Offenhausser, A., 2008. Transmission electron microscopy study of the cell-sensor interface. J. R. Soc. Interface 5 (19), 213–222.
Wu, J., Jiang, S., Xie, W., Xue, Y., Qiao, M., Yang, X., Zhang, X., Wan, Q., Wang, J., Chen, J., Pei, X., 2022. Surface modification of the Ti surface with nanoscale bio-MOF-1 for improving biocompatibility and osteointegration in vitro and in vivo. J. Mater. Chem. B 10 (41), 8535–8548.
Xu, Y., Xie, X., Duan, Y., Wang, L., Cheng, Z., Cheng, J., 2016. A review of impedance measurements of whole cells. Biosens. Bioelectron. 77, 824–836.
Zhou, H.C., Kitagawa, S., 2014. Metal-organic frameworks (MOFs). Chem. Soc. Rev. 43 (16), 5415–5418.